Materials Science Forum Vols. 503-504 (January 2006) pp. 751-756
online at http://www.scientific.net

Nanocrystalline Formation during Mechanical Attrition of Cobalt

J. Zhou[1], C. Sun[1], X. Wu[1,2,a], N. Tao[2,b], G. Liu[2], X. Meng[3], Y. Hong[1,c]

[1]State Key Laboratory of Nonlinear Mechanics, Institute of Mechanics, Chinese Academy of Sciences, Beijing 100080, China

[2]Shenyang National Laboratory for Materials Sciences, Institute of Metal Research, Chinese Academy of Sciences, Shenyang 110016, China

[3]Department of Materials Sciences, Nanjing University, Nanjing 210093, China

[a] xlwu@imech.ac.cn, [b] nrtao@imr.ac.cn, [c] hongys@imech.ac.cn

Keywords: nanostructure, grain refinement, surface mechanical attrition treatment, cobalt

Abstract. The nanocrystalline (nc) formation was studied in cobalt (a mixture of ε (hexagonal close packed) and γ (face-centered cubic) phases) subjected to surface mechanical attrition treatment. Electron microscopy revealed the operation of $\{10\bar{1}0\}\langle 11\bar{2}0\rangle$ prismatic and $\{0001\}\langle 11\bar{2}0\rangle$ basal slip in the ε phase, leading to the successive subdivision of grains to nanoscale. In particular, the dislocation splitting into the stacking faults was observed to occur in ultrafine and nc grains. By contrast, the planar dislocation arrays, twins and martensites were evidenced in the γ phase. The strain-induced γ→ε martensitic transformation was found to progress continuously in ultrafine and nc grains as the strain increased. The nc formation in the γ phase was interpreted in terms of the martensitic transformation and twinning.

Introduction

Severe plastic deformation (SPD) has emerged as a promising method to producing ultrafine and nanocrystalline (nc) materials [1-6]. These materials exhibit superior mechanical properties such as excellent superplasticity, high strength, and good or even excellent ductility [7,8]. SPD is a "top-down" approach for synthesizing ultrafine and nc solids in which existing coarse-grained materials are processed to induce substantial grain refinement and nc formation. The grain refinement is originated from dislocation activity during deformation in cubic metals and alloys with a medium-to-high stacking fault energy (SFE). Plastic straining induces low angle dislocation boundaries which then increase their misorientations with increasing strain to become high angle grain boundaries and as a result, the original grains are subdivided successively down to the nanoscale [9-12]. In this work, the grain refinement and nc formation were studied in low SFE cobalt subjected to surface mechanical attrition treatment (SMAT) [5].

Experimental

The material used in this study was an electrodeposited cobalt plate (purity: 99.98 wt%) with a dimension of 100×40×5 mm^3. The original grain size was determined to be ~30 μm. The X-ray diffraction analysis indicated a duplex ε (hexagonal close packed, hcp) and γ (face-centered cubic, fcc) structure of the product. The volume fraction of γ phase was ~20%. In fact, it is difficult to obtain polycrystalline cobalt with 100% ε phase, and some amount of metastable γ phase always remains at room temperature regardless of the applied treatment [13].

The technique of SMAT was described in detail in our previous papers [5]. In brief, during

the SMAT process, the hardened steel balls of 8 mm in diameter were placed at the bottom of a cylinder-shaped vacuum chamber attached to a vibration generator, with which the balls were resonated. Because of the high vibration frequency of the system, the sample surface was peened repetitively by a large number of balls within a short period of time. Hence, the grains in the treated layer were effectively refined and the grain sizes presented gradient distribution due to the gradient of strain varying from the surface (extremely large) towards the deep matrix (essentially zero) [5]. The deformation microstructure of various grain size regimes could be examined at different levels of strain [11,12]. In the present work, the SMAT process was performed for 50 minutes at room temperature with a vibrating frequency of 50 Hz in a vacuum.

Following SMAT, the microstructure characterization was performed in a transmission electron microscope (TEM, JEM2010F) operated at 200 kV. Both cross-sectional and plane-view thin foils were prepared for TEM observation [14,15].

Experimental results

ε-cobalt

The whole treated layer was ~200 μm thick and the deformation microstructure was examined from the inside towards treated surface. Fig. 1(a) shows the deformation-induced (0001) basal stacking faults (SFs) at the low strain level (~180 μm below treated surface). These SFs are produced by the glide dislocations on basal planes dissociating into Shockley partials bounding an intrinsic SF, i.e. $1/3\langle \bar{1}2\bar{1}0\rangle \rightarrow 1/3\langle 01\bar{1}0\rangle + 1/3\langle \bar{1}100\rangle$ [16]. The inset is the electron diffraction pattern (EDP) with a $[10\bar{1}0]$ zone axis. Fig.1 (b) is a two-beam image of dislocations taken with (0002) beam (~170 μm deep). The basal plane is in the Bragg position (**g**=(0002)) and SFs are out of contrast. Apart from **c**-type dislocations (short segments), all **a** dislocations are in basal planes. In the two-beam image with $(\bar{1}2\bar{1}0)$ beam, however, the SF fringes come onto contrast ($\mathbf{g}\bullet\mathbf{R}\neq 0$, integer) and interfere with the dislocation images. It is, thus, impossible to uniquely identify **a**-type dislocations. However, strong interplay of SFs with dislocations is visible (Fig. 1(a)), indicative of the presence of **a** slip. Hence, the slip of dislocations on pyramidal (**c**+**a**) and basal (**a**) planes occurs in the grains of ε-cobalt.

With increasing strain (~130 μm deep), the low-angle dislocation boundaries present due to dislocation slip. Fig. 2(a) shows the dislocation boundaries oriented normal and parallel to the

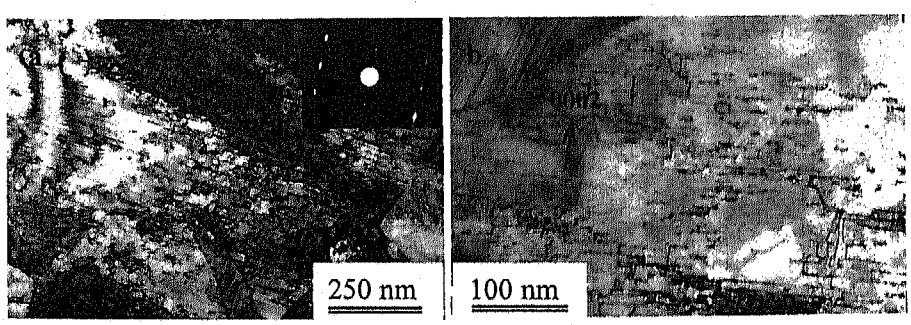

Fig. 1 TEM micrographs. (a) stacking faults and (b) dislocations in ε-phase (~180 μm deep).

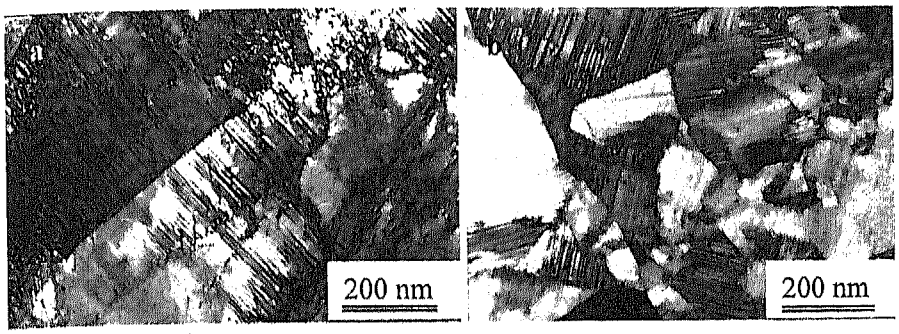

Fig. 2 TEM micrographs. (a) dislocation boundaries (indicated by arrowheads) in the hcp phase (~130 μm deep). (b) Subgrain formation (~130 μm deep).

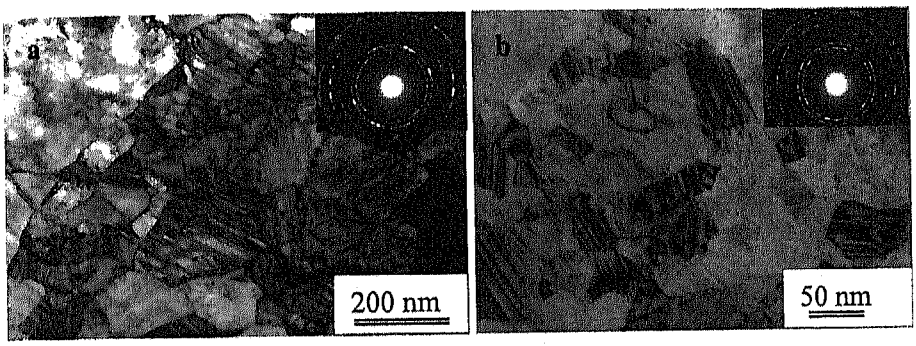

Fig. 3 TEM micrographs. Ultrafine (a) and nanocrytalline (b) grains at ~130 and 30 μm deep respectively.

streaks of SFs, respectively, indicated by a pair of solid and hollow triangles. This indicated the dislocation slip on $\{10\bar{1}0\}$ prismatic and (0001) basal planes respectively [14,17]. Because the direction of dislocation slip was conclusively determined to be $\langle 11\bar{2}0\rangle$ in ε-cobalt [18], the slip system should be prismatic $\langle 11\bar{2}0\rangle\{10\bar{1}0\}$ and basal $\langle 11\bar{2}0\rangle(0001)$. It is worth noting that the SF streaks at one side of dislocation boundary almost disappear. This indicates the presence of the misorientation caused by the dislocation boundary. Fig. 2(b) shows the formation of subgrains due to the subdivision of dislocation boundaries by $\langle 11\bar{2}0\rangle\{10\bar{1}0\}$ prismatic slip.

With successive grain subdivision, the grain refinement continues and hence, the ultrafine and nc grains are formed, as shown in Fig. 3(a) and (b) at ~ 70 and 25 μm deep, respectively. The inset is the EDP consisting of a set of sharp rings, indicating high disorientations among most of grains. The SFs of various orientations are visible in most grains.

γ-cobalt

Fig. 4(a) is a cross-sectional image showing the intersecting planar arrays of dislocations in the grain of γ-cobalt at the low strain level (~170 μm deep). Fig.4 (b) shows twin plates with three {111} orientations, e.g. T_1' and T_1. The inset is the EDP with a [110] zone axis. A decrease in SFE will result in more planar dislocations and twins.

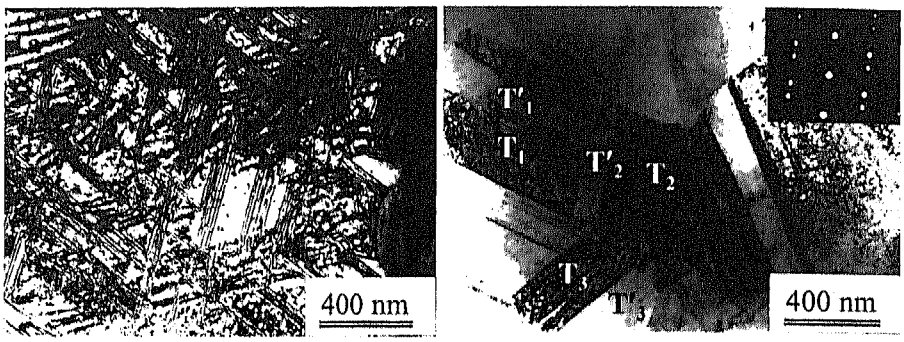

Fig. 4 Planar dislocation arrays (a) and twins (b) in γ-cobalt (~170 μm deep).

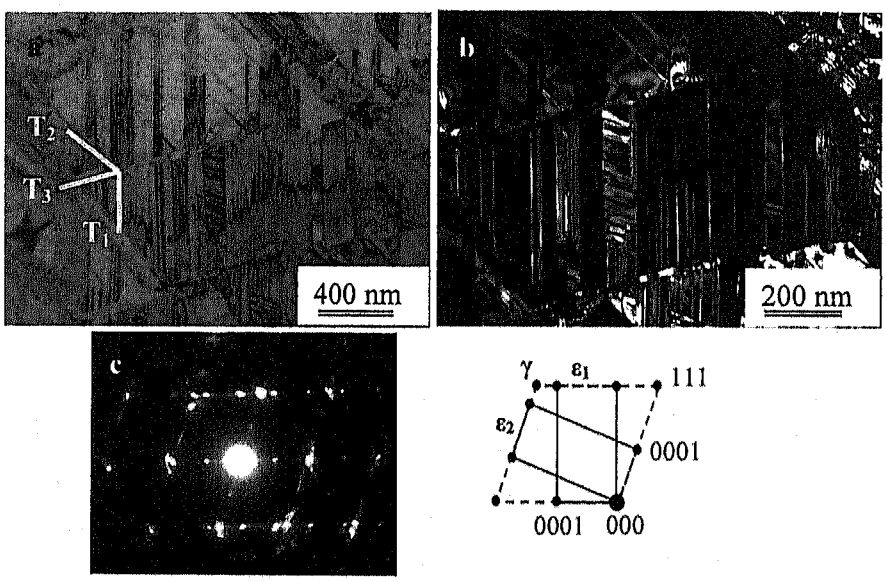

Fig. 5 (a) The intersecting network of ε-martensite platelets on three sets of $\{111\}_\gamma$ planes (~140 μm deep). (b) dark-field image of martensites, (c) EDP and indexing.

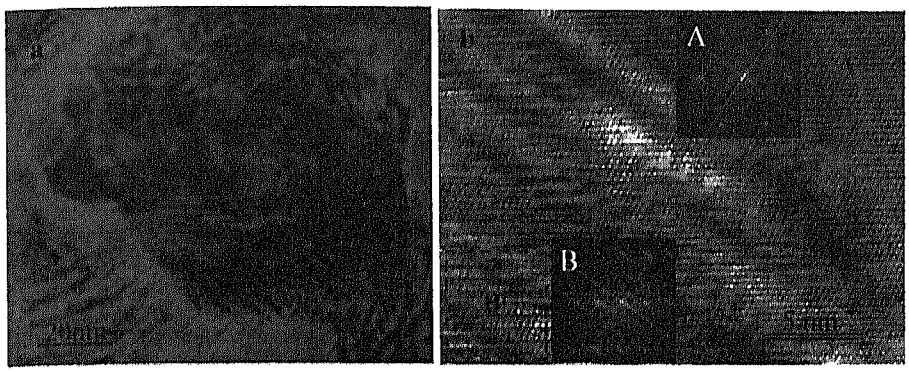

Fig. 6 (a) TEM micrograph of a nc grain. (b) HRTEM lattice image showing the fcc and hcp structure (indicated by square A and B, respectively). Inset is the FFT EDP.

With increasing strain, the strain-induced γ→ε martensitic transformation occurs, as shown in Fig. 5(a). The formation of intersecting networks of ε-martensites on three of four possible sets of $\{111\}_\gamma$ planes is visible (~140 μm deep). The martensites with an orientation of T_1 and T_2 occur in γ between the first set of T_3 orientated martensites. The high magnification dark field image in Fig. 5(b) shows T_1 orientated ε-martensites. Fig. 5(c) was the EDP, consisting of one fcc pattern with a [110] zone axis superimposed on two hcp patterns with $[2\bar{1}\bar{1}0]$ zone axis. The γ→ε transformation results in largely coherent martensite platelets, having the (0001) habit plane and strictly complying with the following orientation relationship, namely $(0001)_\varepsilon$ $//\{111\}_\gamma$ and $\langle 11\bar{2}0\rangle_\varepsilon // \langle 110\rangle_\gamma$.

The γ→ε transformation continues to occur in the nc grain as the strain increases. Fig. 5(a) shows a grain of ~ 80 nm in size. Fig. 5(b) is the lattice image. The fcc and hcp crystal structure is observed as indicated by squares A and B, respectively. Insets (A) and (B) are corresponding fast Fourier transform (FFT) EDPs, with the zone axes [110] and $[2\bar{1}\bar{1}0]$, respectively.

Discussion

The slip of dislocations is the typical character for accommodating strain in ε-cobalt during deformation, similar to that in medium-to-high SFE cubic metals [8-12]. The grain refinement stems from grain subdivision due to $\{10\bar{1}0\}\langle 11\bar{2}0\rangle$ prism and $\{0001\}\langle 11\bar{2}0\rangle$ basal slip. The process of grain subdivision proceeds successively with strain to a finer and finer scale, resulting in the formation of ultrafine and nc grains. It is interest to note the basal SFs inside ultrafine and nc grains. The formation of SFs involves the partial dislocation activity and hence, has a significant effect on deformation especially at nanoscale.

The deformation microstructure in γ-cobalt contains the planar arrays of dislocations, twins, and strain-induced martensites. This is due to that fact that the low SFE γ-cobalt is thermodynamically metastable. Especially, the γ→ε martensite transformation may occur in ultrafine and nc grains as the strain increases. The transformation contributes grain refinement in two respects. First, the transformation results in the formation of refined ε platelets and

second, the ε platelets can be thought of as grain boundaries inducing a refinement effect by subdividing the grains with the same function as deformation twins.

Summary

1. The grain refinement of ε-cobalt is realized through grain subdivision by the $\{10\bar{1}0\}\langle 11\bar{2}0\rangle$ prism and $\{0001\}\langle 11\bar{2}0\rangle$ basal slip. The stacking faults exist in ultrafine and nc grains.

2. The γ-cobalt accommodates strain through dislocation slip, twinning, and strain-induced martensitic transformation. The martensitic transformation proceeds to nanoscale and is responsible for grain refinement of γ-cobalt.

Acknowledgements

This research received backing from the National Basic Research Program of China through Grant No. 2004CB619305, Natural Science Foundation of China Grant No. 50471086, 10472117, and the Chinese Academy of Sciences Grant No. KJCX2-SW-I.2 and National Center for Nanoscience and Technology, China..

References

1. R.Z. Valiev, R.K. Islamgaliev and I.V. Alexandrov. Prog. Mater. Sci. Vol. 45 (2000), p. 103

2. Y.T. Zhu and T.G. Langdon: JOM Vol. 56 (2004), p. 58

3. T.C. Lowe and R.Z. Valiev: JOM Vol. 56 (2004), p. 64

4. M. Furukawa, Z. Horita, T.G. Langdon. Adv. Eng. Mater. Vol. 3 (2001), p. 121

5. K. Lu and J. Lu. J Mater. Sci. Technol. Vol. 15 (1999), p. 193; Mater. Sci. Eng. A Vol. 375-77 (2004), p. 38

6. Y.T. Zhu, T.C. Lowe, T.G. Langdon. Scripta Mater. Vol. 51 (2004), p. 825

7. Z. Horita, T. Fujinami, M. Nemoto, T.G. Langdon. Metall. Mater. Trans. A. Vol. 31 (2000), p. 691

8. J.Y. Huang, Y.T. Zhu, H. Jiang and T.C. Lowe. Acta Mater. Vol. 49 (2001), p. 1497

9. Y. Iwahashi, Z. Horita, M. Nemoto and T.G. Langdon. Acta Mater. Vol. 45 (1997), p. 4733

10. S.D. Terhune, D.L. Swisher, K. Oh-Ishi, Z. Horita, T.G. Langdon and T.R. McNelley. Metall. Mater. Trans. A. Vol. 33 (2002), p. 2173

11. X. Wu, N. Tao, Y. Hong, B. Xu, J. Lu and K. Lu. Acta Mater. Vol. 50 (2002), p. 2075

12. N.R. Tao, Z. Wang, W. Tong, M. Sui, J. Lu and K. Lu. Acta Mater. Vol. 50 (2002), p. 4603.

13. M.J. Bibby and J. Gordon Parr. Cobalt Vol. 20 (1963), p. 111

14. X. Wu, N. Tao, Y. Hong, G. Liu, B. Xu, J. Lu and K. Lu. Acta Mater. Vol. 53 (2005), p. 681

15. X. Wu, N. Tao, Y. Hong, J. Lu and K. Lu. Scripta Mater. Vol. 52 (2005), p. 547

16. C. Hitzenberger, H.P. Karnthaler and A. Korner. Phys. Stat. Sol (a). Vol. 89 (1985), p. 133

17. D.H. Shin, I. Kim, J. Kim, Y.S. Kim and S.L. Semiatin. Acta Mater. Vol. 51 (2003), p. 983

18. M.H. Yoo and C.T. Wei. J App. Phys. Vol. 38 (1967), p. 4317